



Universiteit Utrecht

Binary hard sphere mixtures in gravity

N.A.Keizer

August 19, 2009

Master Thesis

Supervisors:
Prof. dr. ir. M. Dijkstra
Dr. R. van Roij
Drs. M.A.T. Marechal

Faculty of Science
Department of Physics and Astronomy
Soft Condensed Matter

Abstract

In this thesis, floating behavior was investigated in a binary mixture of colloids in a gravitational field. The effects of the size ratio, mass ratio and gravity were determined using density functional theory and a mechanical equilibrium condition.. Monte Carlo simulations were performed to confirm the theories.

Contents

1	Introduction	2
2	Theory & Methods	5
2.1	Test particle theory	5
2.2	The Local Density Approximation	8
2.2.1	Density functional theory	8
2.2.2	Hard spheres in gravity	9
2.2.3	A binary mixture of hard spheres	10
2.2.4	Solving the coupled set of equations	11
2.3	A Free volume-like DFT	11
2.4	Maxwell-Stefan diffusion theory	14
2.4.1	Our approach	15
2.4.2	Biesheuvel's approach	15
2.5	Monte Carlo Simulations	16
2.5.1	The Metropolis Algorithm	16
2.5.2	Modelling a system of binary hard spheres in gravity	16
3	Results & Discussion	19
3.1	Comparison with Literature and Monte Carlo	19
3.1.1	Pure hard spheres	19
3.1.2	Binary	21
3.1.3	Monte Carlo simulations on these parameters	22
3.1.4	Monte Carlo confirmation for more accessible parameters	23
3.2	Test particle theory	24
3.2.1	Checking the theory against LDA calculations	25
3.2.2	Limits of the test particle theory	27
3.3	Results and limits of the simpler theory	29
3.4	Comparison with Biesheuvel	31
4	Conclusion	33

Chapter 1

Introduction

This master thesis focuses on binary systems of hard spheres in an external field. Both Monte Carlo simulations and theoretical calculations were performed to describe the phase behavior of a mixture consisting of two types of hard spheres, varying in size and mass, in a gravitational field. In particular, the floating behavior of large particles in a surrounding sea of smaller particles was investigated.

Such particles are also known as colloids. Colloids are very small particles that have a typical size between 10^{-9} and 10^{-6} meters and are always dissolved in water or oil. Examples of colloidal mixtures are: milk, mayonnaise, blood and jelly. Colloids are thus very common and are used in everyday products.

One of the defining features of colloids is Brownian motion. This effect was discovered by Robert Brown, who observed a jittery motion of pollen grains suspended in water. The same behavior was found with dust particles, ruling out the hypothesis that the pollen were alive. The effect was clearly related to particles with sizes smaller than about a micrometer. This motion is caused by collisions of the particles with micron-sized particles. While individual solvent particles are not visible, their collisions with the colloids and the resulting movement is clearly visible. Particles which undergo Brownian motion are called colloids.

We describe the colloids as hard spheres. These hard spheres are microscopic billiard balls, with no long range interaction and a steep short range repulsion. This is a drastic simplification, since the effect of charges is often important in colloidal mixtures. This simple view does grasp the essence of the problem, allowing us to study the problem in great detail.

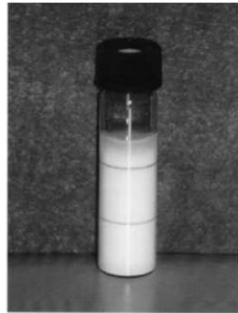
When a suspension of hard spheres is placed in gravity, the particles will sediment to the bottom. A bit like billiard balls in a swimming pool. Billiard balls are so heavy, that they do not experience brownian motion. However, our system does not contain billiard balls, but colloids. The thermal motion which they experience causes them not to completely float to the bottom, but some keep 'jumping' up. An analogy to this is the air. Air molecules do not lie on top of the earth as if they are a sea. The concentration of air particles and thus the pressure, declines as you rise up through the air. The colloids in gravity have a similar behavior.

At the bottom of the suspension, there are thus more colloids than at the top. The average mass density of the suspension is thus not a constant, but

a function of height. At the bottom, the total mass density is higher than at the top. Now, when you place another particle in this suspension with a mass density somewhere between the mass density at the top and at the bottom, it will float somewhere in the middle. In fact, due to Archimedes' principle, it should float at the position where its internal mass density matches that of the surrounding medium.

The first measurements of such a density profile were done in 1910 by Perrin, using a microscope. This allowed him to determine the Boltzmann constant [1]. Recently, such density profiles were calculated using density functional theory and simulations [2, 3, 4, 5] and are measured using light scattering techniques [6, 7] and confocal microscopy [8].

This floating behavior can be used in sedimentation experiments. The speed of the sedimentation of a colloid mixture can be determined by inserting large and thus clearly visible particles with a mass density between the minimum and maximum density of the mixture. Because these particles will float at the height where their internal mass density matches that of the mixture, a clear meniscus will appear. The position of such a meniscus can then be tracked over time to determine a sedimentation speed. An example of such behavior can be seen in figure 1.1 [9]. In the photo, large particles, which are visible to the eye, float at a specific height. Tracer layers of different mass densities float at different heights.



(a)

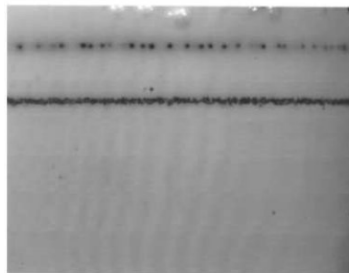


Figure 1.1: *PS (upper) and PMMA (lower) tracer layers in a suspension of α -alumina.* [9]

In this thesis we have investigated how the parameters of the experiment influence the positions of the floating particles. These parameters are the size ratio, the relative mass densities and the effect of gravity. Several different theories were tested against Monte Carlo simulations and each other. In chapter

2, the various theories are described and the methods to extract data from this are briefly explained. In chapter 3, I give the results from the various theories and determine which theory holds when.

Chapter 2

Theory & Methods

For the description of the hard sphere system, a variety of models were used. First a mechanical equilibrium argument, which gives analytic expressions for the location and width of the large particles. Second was a statistical mechanics calculation, using the full chemical potential to obtain numerical density profiles and third, a Monte Carlo simulation which also gave numerical density profiles. For each model, some theoretical background will be given and also the methods used to extract data will be discussed.

2.1 Test particle theory

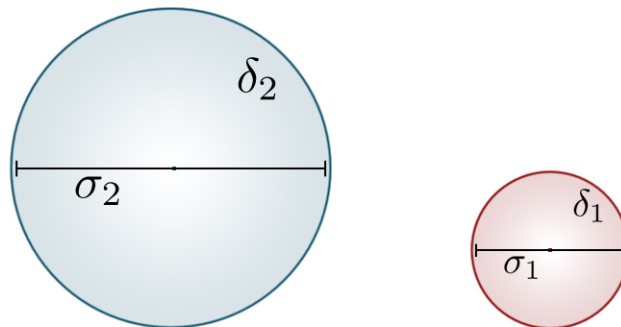


Figure 2.1: Schematic representation of the two types of particles. The small (red) particle has a diameter of $\sigma_1 = 2a_1$ and an internal mass density of δ_1 . The large (blue) particle has a diameter of $\sigma_2 = 2a_2$ and an internal mass density of δ_2 .

In this section we consider the case of one large particle in a background of sedimented smaller particles, where we assume the distribution of small particles to be known. First the use of a buoyant mass will be justified by considering

only the smaller particles and then we will use their pressure to determine the height and width of the large particle distribution.

First, we define mechanical equilibrium for a pure incompressible solvent

$$\frac{dP_0(z)}{dz} = -g\delta_s, \quad (2.1)$$

where δ_s is the mass density of the solvent, $P_0(z)$ the pressure of the solvent at height z and g is the gravitational constant.

We now consider mechanical equilibrium of colloids suspended in this solvent

$$\frac{dP(z)}{dz} = -g\delta(z), \quad (2.2)$$

where P is the total pressure of the solvent and colloids and $\delta(z)$ is the total mass density. Equation (2.2) can then be rewritten in terms of internal mass densities δ_s and δ_1 , for the solvent and colloids respectively, and the volume fraction $\eta_1(z)$ of the colloids. The pressure P is expanded to contain an osmotic pressure term Π which is the pressure caused by the addition of colloids to the system

$$\begin{aligned} \frac{dP(z)}{dz} &= -g\delta(z) \\ &= -g((1 - \eta_1(z))\delta_s + \eta_1(z)\delta_1) \\ &= -g(\delta_s + \eta_1(z)(\delta_1 - \delta_s)) \end{aligned} \quad (2.3)$$

$$\equiv \frac{d(P_0(z) + \Pi(z))}{dz}. \quad (2.4)$$

From Eq. (2.3) and (2.4) with Eq. (2.1) it follows that

$$\begin{aligned} \frac{d\Pi(z)}{dz} &= -g\eta_1(z)(\delta_1 - \delta_s) \\ &= -g\rho_1(z)(\delta_1 - \delta_s)v_1 \\ &= -gm_1\rho_1(z), \end{aligned} \quad (2.5)$$

where m_1 is defined by $(\delta_1 - \delta_s)v_1$ which is equal to $M_1 - v_1\delta_s$, the buoyant mass. Here $v_1 = \frac{4\pi}{3}a_1^3$ is the volume of a single particle with radius a_1 , M_1 its mass and $\rho_1(z)$ is the number density. The osmotic pressure is thus only influenced by the buoyant mass of the particles.

We now add a single large particle of radius a_2 and mass density δ_2 and determine the force $\vec{F}_{1s2}(z)$ exerted on this particle by the solvent and the small colloids. The pressure is integrated over a sphere with radius $a_1 + a_2$, because this is typical distance at which the large colloid interacts with the smaller colloids.

$$\begin{aligned}
\hat{z} \cdot \vec{F}_{1s2}(z) &= - \int d\hat{n} (a_1 + a_2)^2 P(z + (a_1 + a_2)\hat{n} \cdot \hat{z})(\hat{z} \cdot \hat{n}) \\
&= -(a_1 + a_2)^2 \int d\hat{n} \left(P(z) + ((a_1 + a_2)\hat{n} \cdot \hat{z}) \frac{dP(z)}{dz} + \mathcal{O}((\hat{n} \cdot \hat{z})^\epsilon) \right) (\hat{z} \cdot \hat{n}) \\
&= -(a_1 + a_2)^3 \frac{dP(z)}{dz} \int d\hat{n} (\hat{z} \cdot \hat{n})^2 \\
&= -\frac{4\pi}{3} (a_1 + a_2)^3 \frac{dP(z)}{dz}. \tag{2.6}
\end{aligned}$$

Here we have ignored the terms involving higher order derivatives of the pressure. The integral over $P(z)$ is antisymmetric and hence zero, so that this term drops out of the equation. This implies that the force on the large particle is determined by the derivative of the pressure from the smaller particles. We can consider the force on particle 2 to be due to a potential energy term. Because $\hat{z} \cdot \vec{F}_{12}(z) \equiv -\frac{dW_2(z)}{dz}$, this potential energy due to the presence of the solvent and small colloids is given by

$$W_2(z) = C + \tilde{v}P(z), \tag{2.7}$$

where \tilde{v} is defined as $\frac{4\pi}{3}(a_1 + a_2)^3$ and C is an integration constant. Using the potential energy of particle 2 due to gravity $W_{2,grav}(z) = M_2gz$, yields the total potential energy of particle 2

$$W(z) = W_{2,grav}(z) + W_2(z). \tag{2.8}$$

The equilibrium position z^* of particle 2 can be determined from the equilibrium condition, that the derivative of the total potential energy of particle 2 is zero. Using Eq. (2.3), we find

$$\begin{aligned}
0 &= \left. \frac{dW(z)}{dz} \right|_{z=z^*} \\
&= \tilde{v} \frac{dP(z)}{dz} + M_2g \\
&= \tilde{v} (-g\delta_s - g\eta_1(z) (\delta_1 - \delta_s)) + M_2g.
\end{aligned}$$

Defining the adjusted mass density of the larger particle $\tilde{\delta} = \frac{M_2}{\tilde{v}}$. we find

$$\tilde{\delta} = (1 - \eta_1(z)) \delta_s + \eta_1(z) \delta_1, \tag{2.9}$$

Because \tilde{v} is larger than v_2 due to the fact that the radius is $a_1 + a_2$ instead of a_2 , the large particle gets a lower effective mass density. If the volume fraction distribution is known, solving equation 2.9 for z will determine the height z^* at which the larger particles will float. If $a_2 \gg a_1$, $a_1 + a_2 \approx a_2$, so for very large particles, the position at which they will float is when their internal mass density becomes equal to the mass density of the surrounding medium, so small particles plus solvent. This principle is widely used and also known as Archimedes' Principle. However, when the particle radii are about the same

size, the larger particle will have a smaller effective mass density, thus floating higher than one would expect.

A Taylor expansion can be used at $z = z^*$ to expand the potential energy up to its second derivative. Using $\left. \frac{d^2 W(z)}{dz^2} \right|_{z=z^*} = \tilde{v} \frac{d^2 P(z)}{dz^2} = -m_1 g \tilde{v} \rho_1'(z^*)$,

$$W(z) = W(z^*) + \frac{1}{2} (z - z^*)^2 \left. \frac{d^2 W(z)}{dz^2} \right|_{z=z^*} \quad (2.10)$$

$$= W(z^*) - \frac{1}{2} m_1 g \tilde{v} \rho_1'(z^*) (z - z^*)^2, \quad (2.11)$$

since the first derivative of the potential energy vanishes at z^* . Because the density of the large particles is low, they can be described by an ideal gas in an external field and we can add the potential energy to the chemical potential to obtain the distribution of the large particle,

$$\ln \rho_2(z) + \beta W(z) = \beta \mu. \quad (2.12)$$

Which gives

$$\rho_2(z) \propto \exp(-\beta W(z)) \quad (2.13)$$

$$\propto \exp\left(\frac{1}{2} \beta m_1 g \tilde{v} \rho_1'(z^*) (z - z^*)^2\right), \quad (2.14)$$

i.e. a Gaussian distribution of the position of the large particle around its height z^* with a width

$$\sigma = \langle (z - z^*)^2 \rangle^{1/2} = \sqrt{\frac{-k_B T}{m_1 g \tilde{v} \rho_1'(z^*)}}. \quad (2.15)$$

of the particle distribution. Upon increasing the gravitational strength, the volume of particle 2 or the steepness of the density profile of the small particles, the density distribution of the large particle becomes narrower. This equation and also equation (2.9) will be checked against numerical data in section 3.2.

2.2 The Local Density Approximation

2.2.1 Density functional theory

For the theoretical description of the mixture consisting of 2 types of hard spheres in a gravity field, density functional theory (DFT) was used. This theory is an extension of classic statistical physics. This is done by replacing the number density ρ by a positional dependent $\rho(z)$ and by using the intrinsic Helmholtz free energy functional $F[\rho_0]$ instead of considering the Helmholtz free energy $F(N, V, T)$. By functional minimization of the grand potential, the number density is determined. This minimization can be rewritten in terms of the free energy functional as

$$\left. \frac{\delta F[\rho]}{\delta \rho(\vec{r})} \right|_{\rho_0(\vec{r})} = \mu - V_{\text{ext}}(\vec{r}), \quad (2.16)$$

where $V_{\text{ext}}(\vec{r})$ is the external potential, i.e. an electric field or gravity and μ is the total chemical potential. The obtained equilibrium number density $\rho_0(\vec{r})$

will be a unique function, depending on F and V_{ext} . However, it is nearly impossible to determine the free energy functional explicitly for non-ideal cases and often an approximation has to be made. The approximation used in this thesis is the local density approximation (LDA). The free energy functional is approximated using the free energy of the bulk system by

$$F[\rho(\vec{r})] = \int d\vec{r} f(\rho(\vec{r}), T) \quad (2.17)$$

where $f(\rho, T) = F(N, V, T)/V$ is the free energy per unit volume of the system and $\rho = N/V$. The LDA is very useful to model systems with low density fluctuations, because in the integral, nearby densities are not considered, only those at \vec{r} . This is a poor model for systems with interfaces, because the rapid fluctuations are not incorporated. In our hard sphere model, we only expect rapid fluctuations as at the bottom due to the layering of the particles, but the physics of interest for us happens above the layering where the LDA can be safely used.

2.2.2 Hard spheres in gravity

Before tackling the binary mixture problem, the LDA will be applied to a one component fluid, from which the binary mixture will be a natural extension. Let N be the number of particles with diameter σ . These particles are contained in a box with size $V = A \times L$, where A is the surface area and L the height of the box. The potential energy of a particle i in an external gravitational field reads

$$V_{\text{ext}}(z_i) = mgz_i, \quad (2.18)$$

where m is the buoyant mass of the particles, g the gravitational constant and z_i the height. The density profiles $\rho(z)$ induced by gravity are normalized by

$$n = \frac{1}{L} \int_0^L dz \rho(z) \quad (2.19)$$

where $n = N/V$, the average number density in the box. Because we are interested in the overall shape of the density profile we can use the LDA to obtain it. In particular, we are not interested in the layering that occurs at the bottom of the box, which the LDA cannot describe, since it is a local density approximation. The free energy functional of hard spheres in the LDA is

$$F[\rho] = \int_0^L dz (f_{\text{id}}[\rho, T] + f_{\text{exc}}^{HS}[\rho, T]) \quad (2.20)$$

Taking the functional derivative with respect to the local density and inserting it into Eq. (2.16) gives

$$\mu_{\text{id}}(\rho(z)) + \mu_{\text{exc}}^{HS}(\rho(z)) = \mu - V_{\text{ext}}(z). \quad (2.21)$$

The chemical potential of a hard sphere system can be approximated using the Percus Yevick approximation followed by a linear combination of the virial and compressibility routes, i.e., the Carnahan Starling expression. This results in

$$\beta\mu_{\text{id}} + \beta\mu_{\text{exc}}^{HS} = \beta\mu^{HS} = \log(\rho\Lambda^3) + \frac{3\eta^3 - 9\eta^2 + 8\eta}{(1-\eta)^3} \quad (2.22)$$

where $\eta = \frac{\pi}{6}\sigma^3\rho$ is the volume fraction, Λ is the thermal wavelength and $\beta = 1/(k_bT)$. Equations (2.21) and (2.22) can be combined into a local equation

$$\eta(z) = \frac{\frac{\pi}{6}\sigma^3}{\Lambda^3} \exp\left(\beta\mu - \beta mgz - \frac{3(\eta(z))^3 - 9(\eta(z))^2 + 8\eta(z)}{(1-\eta(z))^3}\right). \quad (2.23)$$

This equation can be solved numerically by a simple bisection root finding algorithm. For instance, if the logarithm of equation 2.23 is taken and is rewritten to

$$\log(\eta(z)) - \beta\mu + \beta mgz + \frac{3\eta(z)^3 - 9\eta(z)^2 + 8\eta(z)}{(1-\eta(z))^3} = 0, \quad (2.24)$$

where we have absorbed the prefactor $\frac{\pi}{6}\sigma^3/\Lambda^3$ into $\beta\mu$, we find that the volume fraction profile $\eta(z)$ is a monotonically decreasing function with height z , as expected.

2.2.3 A binary mixture of hard spheres

We now consider a binary mixture of hard spheres as in Ref. [3]. To describe the colloid mixture, we characterize the system with N_1 the number of particles with mass m_1 and diameter σ_1 and N_2 the number of particles with mass m_2 and diameter σ_2 . The particles are enclosed in a box with volume $V = A \times L$, where A is the surface area and L is the vertical height of the box. The size ratio is defined as $y = \sigma_1/\sigma_2 \leq 1$, where species 2 has a larger diameter. In absence of gravity, the number densities are given by $n_i = N_i/V$.

The effect of gravity is incorporated by an external field,

$$V_{\text{ext},i}(z_i) = m_i g z_i \quad (2.25)$$

where m_i is the buoyant mass of particle i , g is the gravitational constant and z_i is the height of particle i in the vertical direction.

Due to this external field the system is inhomogeneous and is characterized by density profiles $\rho_1(z)$ and $\rho_2(z)$ which satisfy the normalization conditions

$$\frac{1}{L} \int_0^L dz \rho_i(z) = n_i. \quad (2.26)$$

As in the pure case, we assume that the density profiles vary slowly compared to the particle diameter, so that we can use the local density approximation. This results in the free energy functional

$$F[\rho_1(z), \rho_2(z)] = \int_0^L dz f_{\text{id}}[\rho_1(z), \rho_2(z), T] + \int_0^L dz f_{\text{ext}}[\rho_1(z), \rho_2(z), T]. \quad (2.27)$$

Taking the functional derivative of Eq. (2.27) to $\rho_i(z)$ gives

$$\mu_{\text{id},i}(\rho_i(z), T) + \mu_{\text{exc},i}^{HS}(\rho_1(z), \rho_2(z), T) = \mu_i - V_{\text{ext},i}(z), \quad (2.28)$$

where we take the Mansoori Carnahan Starling chemical potential for hard spheres mixtures [10] for μ_{exc}^{HS} . Because $\mu_{\text{id}}(\rho_i(z), T) = k_B T \log(\rho_i(z)\Lambda_i^3)$ this can be inserted into Eq. (2.28) to obtain the local equations

$$\rho_i(z) = \frac{1}{\Lambda_i^3} \exp(\beta\mu_i - \beta V_{\text{ext},i}(z) - \beta\mu_{\text{exc},i}^{HS}(\rho_1(z), \rho_2(z), T)) \text{ for } i \in \{1,2\}. \quad (2.29)$$

Solving this is not as trivial as in the pure case because it is a coupled set of equations and a higher dimensional root finding algorithm is computationally demanding.

2.2.4 Solving the coupled set of equations

We start of by rewriting equations (2.29) into the form $f(x) = x$. All number densities are converted to volume fractions.

$$\eta_1(z) = \exp(C_1 - \beta m_1 g z - \beta\mu_{\text{exc},1}^{HS}(\eta_1(z), \eta_2(z), T)) \quad (2.30)$$

$$\eta_2(z) = \exp(C_2 - \beta m_2 g z - \beta\mu_{\text{exc},2}^{HS}(\eta_1(z), \eta_2(z), T)) \quad (2.31)$$

Since beforehand the chemical potential is undetermined and the total volume fraction is known, an additional condition is made

$$\frac{1}{L} \int_0^L dz \eta_i(z) = \eta_{i,\text{tot}}, \quad (2.32)$$

which determines the chemical potential.

Next, an initial guess is made for both packing fraction profiles. These are then inserted into the right hand side of equations (2.30) and (2.31) where C_1 and C_2 are adjusted so that the profiles are normalized according to equation (2.32). These new profiles are again inserted into the right hand side and this process is repeated until the difference between two subsequent profiles becomes sufficiently small or a fixed number of iterations is reached.

One iteration can unfortunately give values of η which are larger than 1.0. The chemical potential is not defined for these values of η , so this must be avoided. This is done by only adding a fraction of the new profile to the previous, so that each new profile is a linear combination of the previous profile and the calculated one.

This process is repeated until the difference between two subsequent profiles becomes sufficiently small or a fixed number of iterations is reached.

2.3 A Free volume-like DFT

A slightly more intuitive way of looking at the mixture is by no longer using the chemical potential for a binary mixture and by using the single mixture hard sphere chemical potential and some approximations instead. This approximation is that the large particles essentially do not feel the smaller spheres and

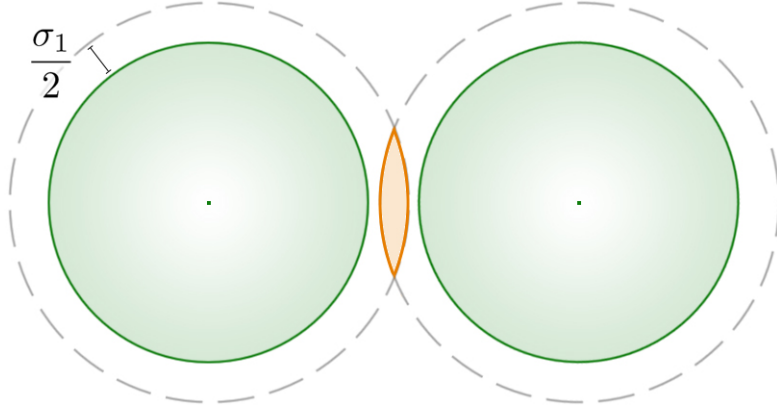


Figure 2.2: Schematic representation of two large particles. The area within the grey dashed lines represents the excluded volume $v_{LS} = \frac{\pi}{6} \left(\frac{\sigma_1 + \sigma_2}{2} \right)^3$ for the smaller particles. When two large particles are close, their excluded volume may overlap (indicated by the orange area). This causes a decrease in the total excluded volume, but the effect is not incorporated in the simplified DFT.

that the small particles cannot be at the same place as the large particles by means of an excluded volume term. This stems from the following derivation, which starts from the canonical partition function of the binary mixture in the bulk

$$Z = \exp(-\beta F_{\text{mix}}) = \frac{1}{\Lambda_L^{3N_L} N_L!} \frac{1}{\Lambda_S^{3N_S} N_S!} \int dr_L^{N_L} \int dr_S^{N_S} \exp(-\beta[\Phi_{SS} + \Phi_{LL} + \Phi_{SL}]), \quad (2.33)$$

where Λ_S and Λ_L are the thermal wavelengths of the small and large particles respectively, β the inverse temperature, Φ_{SS} the potential governing the small particle interaction, Φ_{LS} the interspecies interaction and Φ_{LL} the large particle interaction. Due to the hard sphere nature of the particles, the interspecies interaction causes a volume where the small particles can not be, since it is occupied by large particles. So now the integral over the small particles changes into the following equation

$$\exp(-\beta F_{\text{mix}}) = \frac{1}{\Lambda_L^{3N_L} N_L!} \int dr_L^{N_L} \frac{\exp(-\beta\Phi_{LL})}{\Lambda_S^{3N_S} N_S!} \int_{V - V_{\text{excluded}}(r_L^{N_L})} dr_S^{N_S} \exp(-\beta\Phi_{SS}). \quad (2.34)$$

Now that the integrals have been separated, they can be written in the form of free energies to obtain the mixing free energy F_{mix} from the partition function. The excluded volume can be approximated by $V_{\text{excluded}} = v_{LS} N_L$. Every large

particle excludes a volume for the smaller particles. This approximation thus ignores an overlap in excluded volume and a possible restructuring of small particles at the edges of the excluded large particle volume.

$$Z = \exp(-\beta F_{\text{mix}}) \approx \exp(-\beta F_{CS}(N_L, V, T)) \exp(-\beta F_{CS}(N_S, V - v_{LS}N_L, T)) \quad (2.35)$$

This results in the following mixing free energy

$$F_{\text{mix}} \approx F_{CS}(N_L, V, T) + F_{CS}(N_S, V - v_{LS}N_L, T) \quad (2.36)$$

$$= V \left(f_{CS}(\rho_L, T) + \frac{V - v_{LS}N_L}{V} f_{CS}\left(\frac{\rho_S}{1 - v_{LS}\rho_L}, T\right) \right), \quad (2.37)$$

where $\rho_L = \frac{N_L}{V}$, $\rho_S = \frac{N_S}{V}$, v_{LS} the excluded volume of a large sphere for a small sphere and ρ_L the volume fraction of the large particles and $f(\rho, T) = \frac{F(N, V, T)}{V}$.

Again the local density approximation is used to obtain the intrinsic free energy

$$F[\rho_S, \rho_L] = \int dr \left(f_{CS}(\rho_L, T) + (1 - v_{LS}\rho_L) f_{CS}\left(\frac{\rho_S}{1 - v_{LS}\rho_L}, T\right) \right) \quad (2.38)$$

Taking the functional derivative then gives the conditions for the density profiles. The first condition is given by

$$\frac{\delta F}{\delta \rho_S(r)} = \frac{1 - v_{LS}\rho_L}{1 - v_{LS}\rho_L} \mu_{CS}\left(\frac{\rho_S}{1 - v_{LS}\rho_L}, T\right) = \mu_1 - m_S g z \quad (2.39)$$

and the other can be obtained from

$$\begin{aligned} \frac{\delta F}{\delta \rho_L(r)} &= \mu_{CS}(\rho_L, T) - v_{LS} f_{CS}\left(\frac{\rho_S}{1 - v_{LS}\rho_L}, T\right) + \\ &\quad (1 - v_{LS}\rho_L) \mu_{CS}\left(\frac{\rho_S}{1 - v_{LS}\rho_L}, T\right) \rho_S v_L (1 - v_{LS}\rho_L)^{-2} \end{aligned} \quad (2.40)$$

$$\begin{aligned} &= \mu_{CS}(\rho_L, T) + \\ &\quad v_{LS} \left(-f_{CS}\left(\frac{\rho_S}{1 - v_{LS}\rho_L}, T\right) + \frac{\rho_S}{1 - v_{LS}\rho_L} \mu_{CS}\left(\frac{\rho_S}{1 - v_{LS}\rho_L}, T\right) \right) \end{aligned} \quad (2.41)$$

$$= \mu_{CS}(\rho_L, T) + v_{LS} P_{CS}\left(\frac{\rho_S}{1 - v_{LS}\rho_L}, T\right) = \mu_2 - m_L g z. \quad (2.42)$$

$$(2.43)$$

These can then be inverted to obtain the density profiles

$$\frac{\rho_S}{1 - v_{LS}\rho_L} = \mu_{CS}^{-1}(\mu_1 - m_S g z) \quad (2.44)$$

$$\rho_L = \mu_{CS}^{-1}(\mu_2 - m_L g z - v_L P_{CS}\left(\frac{\rho_S}{1 - v_{LS}\rho_L}, T\right)) \quad (2.45)$$

Two effects can be noted from this. First, the density profiles of the small particles is nearly identical to that in the single mixture, except for a factor

$(1 - v_{LS}\rho_L)$, which 'pushes' the small particles away. The other effect is that a pressure term appears in the equation for the density profiles of the large particles, similar to the test particle theory and also similar to Biesheuvels approach, but slightly different.

2.4 Maxwell-Stefan diffusion theory

Another approach to the binary mixture is by making use of the Maxwell-Stefan theory for mass transfer [11]. This diffusion theory is an improvement of Fick's law which can take the thermodynamical properties and external fields into account. In this theory the driving forces on the particle species are given by the negative gradient of the chemical potential of that species. This means that particles tend to move from high to low chemical potential.

Taking external forces into account, this force is defined by:

$$\rho_i RT d_i \equiv -\rho_i \nabla_T \mu_i + m_i \rho_i \tilde{\mathbf{F}}_i \quad (2.46)$$

Here ρ_i is the particle concentration or number density, R the gas constant, T is temperature, d_i the diffusion force, $\nabla_T \mu_i$ the chemical potential gradient at fixed temperature, m_i the particle mass and $\tilde{\mathbf{F}}_i$ the force per kg of species i . Under the assumption that mechanical equilibrium is obtained,

$$-\frac{1}{\rho_t} \nabla P + \sum_{i=1}^n \omega_i \tilde{\mathbf{F}}_i = 0 \quad (2.47)$$

where P is the pressure, ρ_t the total mass density and ω_i is the mass fraction, equation 2.47 can be added to 2.46 to get

$$\rho_i RT d_i \equiv -\rho_i \nabla_T \mu_i + m_i \rho_i \tilde{\mathbf{F}}_i + m_i \rho_i \left(-\frac{1}{\rho_t} \nabla P + \sum_{i=1}^n \omega_i \tilde{\mathbf{F}}_i \right). \quad (2.48)$$

Then the chemical pressure gradient is expanded to include a pressure term

$$\nabla_T \mu_i = \nabla_{T,P} \mu_i + \bar{V}_i \nabla P. \quad (2.49)$$

where \bar{V}_i is the partial molar volume $\left(\frac{\delta V}{\delta N_i} \right)_{T,P,N_{i \neq j}}$ and $\nabla_{T,P} \mu_i$ the chemical potential gradient at constant temperature and pressure. This is included into 2.48 and after some rewriting we obtain

$$\rho_i k_B T d_i \equiv -\rho_i \nabla_{T,P} \mu_i - (\rho_i \bar{V}_i - \omega_i) \nabla P + m_i \rho_i \left(\tilde{\mathbf{F}}_i - \sum_{k=1}^n \omega_k \tilde{\mathbf{F}}_k \right) \quad (2.50)$$

Now we can apply the theory to the case of a binary hard sphere mixture in gravity. Since we are dealing with a mixture in thermodynamic equilibrium, the diffusion forces are set to zero. The external forces are gravitational, so the force per kilogram is simply $-g$, the gravitational constant. The vanishing term that was included can be taken out again. This results in

$$0 = -\rho_i \nabla_{T,P} \mu_i - \rho_i \bar{V}_i \nabla P - m_i \rho_i g. \quad (2.51)$$

2.4.1 Our approach

Equation can be shown to be equivalent to our DFT approach, by simply not doing the expansion of the chemical potential. This results in

$$\nabla_T \mu_i = -m_i g \quad (2.52)$$

Integrating this equation over z from 0 to z' results in

$$\mu_i(z') = \mu_i(0) - m_i g z'. \quad (2.53)$$

Equation 2.53 is found to be the same as equation 2.28, which shows that Maxwell-Stefan diffusion theory is equivalent to the Local Density approximation for this problem.

2.4.2 Biesheuvel's approach

In the article by Biesheuvel *et al.* [12], a different approach is taken. The starting point is equation 2.50. Then the observation is made that in mechanical equilibrium,

$$\frac{dP}{dh} = \rho_t \sum_j \omega_j F_j. \quad (2.54)$$

Here $\rho_t = \sum_i \eta_i \delta_i + (1 - \eta_i) \delta_L$ is the total mass density, ω_i the mass fraction of particle species i , δ_i the internal mass density of particle species i and η_i its packing fraction. After inserting equation 2.54 and some rewriting, equation 2.50 becomes

$$-d_i = \nabla_{T,P} \mu_i + \bar{V}_i \nabla P + m_i g. \quad (2.55)$$

Dropping the constant T and P restrictions results in

$$-d_i = \frac{d\mu_i}{dh} + \bar{V}_i \frac{dP}{dh} + m_i g. \quad (2.56)$$

Ignoring an external chemical potential, meaning that $\mu_i = \log \phi_i$ and substituting $\frac{dP}{dh} = -\rho_t g$, results in

$$-d_i = \frac{d \log \phi_i}{dh} + m_i^b g, \quad (2.57)$$

with a buoyant mass

$$m_i^b = v_i (m_i \rho_i - \rho_t). \quad (2.58)$$

Here the partial molar volume \bar{V}_i is replaced by the volume v_i of a particle. It is unclear to us if this is allowed. From equation 2.57, it is then argued the gravitational action is based on a buoyant mass defined by the difference in mass density between the particle and its total surrounding medium ($m_i \rho_i - \rho_t$), instead of between the mass density of the particle and the solvent ($m_i \rho_i - \rho_L$). However, this argument is based on the expansion of the chemical potential in equation 2.49, which is not done in our work. Therefore Biesheuvel should use the derivative of the chemical potential under constant pressure and temperature, but it is not clear from the article if he does this.

2.5 Monte Carlo Simulations

Monte Carlo methods are techniques that rely on random number generators to obtain results. What this implies is that you can use a random number generator to create a random walk through phase space (the collection of all available states) to get as many of these states as possible from which you can then obtain the thermodynamics of the system. Because you want to create as many states as possible, computers are very well suited for these calculations.

A statistical average of a measurable quantity Q is then determined by

$$\langle Q(\vec{r}^N) \rangle = \frac{\int d\vec{r}^N Q(\vec{r}^N) \exp[-\beta E(\vec{r}^N)]}{\int d\vec{r}^N \exp[-\beta E(\vec{r}^N)]}, \quad (2.59)$$

where $\beta = 1/(k_B T)$ the inverse temperature, E the energy and \vec{r}^N the positions of all particles. How much an individual state contributes to the statistical average is determined by its energy. By giving all states an equal probability to occur, there will be a lot of states with a relatively high energy, wasting precious computer time on calculations that have no large influence on the result.

2.5.1 The Metropolis Algorithm

One way to prevent wasting time on states that have a negligible contribution is by making use of the Metropolis algorithm [13]. Instead of allowing all states to occur at an equal probability, we bias the random walk so that states with a lower energy - and thus higher contribution - occur more often than those with higher energy. This breaks the condition that every state has an equal probability, but we evade that by computing the statistical average in a different way. The defining feature of a Metropolis algorithm is the acceptance ratio used, which is

$$A(\mu \rightarrow \nu) = \begin{cases} \exp(-\beta(E_\nu - E_\mu)) & \text{if } E_\nu - E_\mu > 0 \\ 1 & \text{otherwise} \end{cases} \quad (2.60)$$

Every state that is generated with a lower energy than the previous state, is accepted, while a state with a higher energy has a probability to be accepted based on the energy difference $E_\nu - E_\mu$ and inverse temperature β . This acceptance ratio is chosen in such a way that a high acceptance rate is ensured and the thermodynamics of the system is kept intact. The statistical average of a measurable quantity Q is now determined by the simple average,

$$\langle Q \rangle = \frac{1}{M} \sum_{i=1}^M Q_i. \quad (2.61)$$

For a detailed explanation read the book by Newman and Barkema [14].

2.5.2 Modelling a system of binary hard spheres in gravity

System parameters

The model describes a system of N_l large particles with diameter σ_l and mass m_l and N_s small particles with diameter σ_s and mass m_s , bound in a 'box' with possible coordinates $(x, y, z) \in [0, a) \times [0, b) \times [0, \infty)$. Periodic boundary

conditions are imposed in the x and y directions. Particles have a gravitational energy $V = m_i g z$ with g the gravitational constant and a hard sphere potential

$$\phi(r_{i,j})_{i,j} = \begin{cases} 0 & \text{if } r_{i,j} > (\sigma_i + \sigma_j)/2, \\ \infty & \text{if } r_{i,j} \leq (\sigma_i + \sigma_j)/2 \end{cases} \quad (2.62)$$

with $i, j \in (1, 2)$.

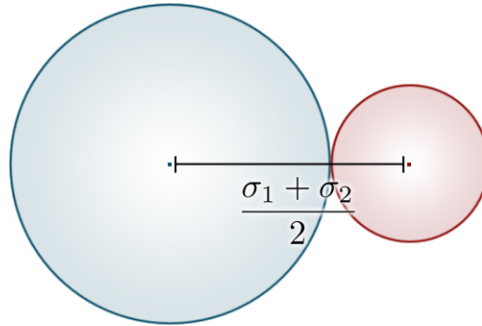


Figure 2.3: Schematic representation of a large (blue) and a small (red) particle. Overlap occurs when the distance between the two particles becomes less than $(\sigma_1 + \sigma_2)/2$.

The simulation in a nutshell

The first step of a simulation is generating an initial state. It should not matter how this is done, because this state will be forgotten and will not be used in measurements. However, a good choice of initial state will make equilibration go faster. My first choice was a completely random system, however after problems with equilibration, the small particles were put randomly into the bottom half of the box and the large particles were put in randomly in the top half.

New states are generated by a random walk. First a particle is chosen at random. Its position is then altered by adding a random step in the x , y and z directions, delimited by the stepsize δ in each direction. This then gives us a new state.

Next up is the decision to accept or reject this new state. This is done via the Metropolis algorithm 2.60. It is easy to see that two overlapping hard spheres generate infinite energy and such a state is therefore always rejected. Particles can also not fall through the floor, so if a particle intersects the xy -plane, the new state is also rejected. Suppose that the move has not caused problems with overlap or the floor. The metropolis algorithm is now invoked again, where the energy difference is determined by the size of the step in the z -direction.

If the state was rejected, we keep the old state and try a different move. If the state was accepted, it becomes the old state and we try a different move.

Obtaining the density profile

Once the system has achieved equilibrium, we wish to obtain the density profile $\rho(z) = \frac{1}{A} \langle \sum_i \delta(z - z_i) \rangle$. The z -positions of the particles are regularly binned and then averaged.

Cell lists

Cell lists are a method to speed up the simulation. Whenever a particle is moved, all other particles must be checked for overlap. For very large systems, this can take a while. A cell list is a list which optimizes the search for overlapping particles. The simulation volume is divided in boxes with a size slightly larger than the radius of the overlap check. The cell list keeps track of which particle is in which box. So when a particle is moved, you only have to check the particles in nearby boxes, instead of checking all particles.

Chapter 3

Results & Discussion

3.1 Comparison with Literature and Monte Carlo

3.1.1 Pure hard spheres

Two different approaches were used to make sure the programs were giving correct output. The first is a direct comparison with literature. The second a comparison between the Monte Carlo simulations and the LDA calculations. In this section the first approach is described.

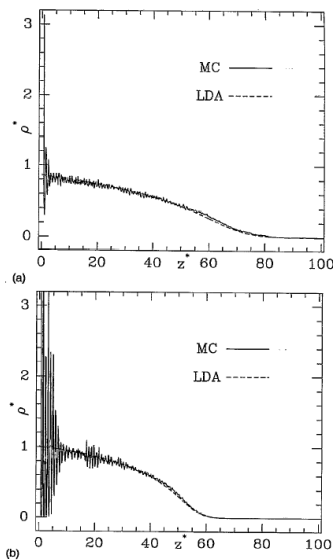


FIG. 2. Reduced density profile $\rho^*(z) = \rho(z)\sigma^3$ of a hard sphere system vs reduced altitude z/σ , for $n_s^* = 40$ and (a) $\alpha^* = 0.2$ and (b) $\alpha^* = 0.4$. The solid curves are Monte Carlo data; the dashes represent the LDA results.

Figure 3.1: *Reduced density profile $\rho^*(z) = \rho(z)\sigma^3$ of a hard spheres system against reduced altitude z/σ , for $n_s^* = 40$ and (a) $\alpha^* = 0.2$ and (b) $\alpha^* = 0.4$. The solid curves are Monte Carlo data; the dashed lines represent the LDA results.*

The first version of the LDA program, where density profiles for a one com-

ponent system of hard spheres in gravity was calculated, was checked against Ref. [2]. The results of the first program were then compared to figure 3.1, using the same parameters. In Ref. [2], Monte Carlo results were used to check the LDA data and were found to match. In this work, this has also been done, giving a first confirmation that the Monte Carlo code and the LDA are correct.

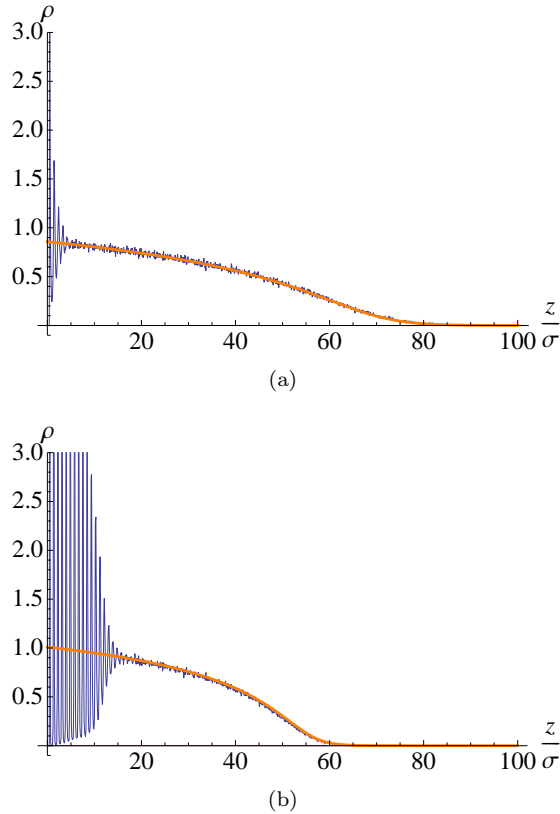


Figure 3.2: *Reduced density profile $\rho^*(z) = \rho(z)\sigma^3$ of a hard spheres system against reduced altitude z/σ , for $n_s^* = 40$ and (a) $\alpha^* = 0.2$ and (b) $\alpha^* = 0.4$.*

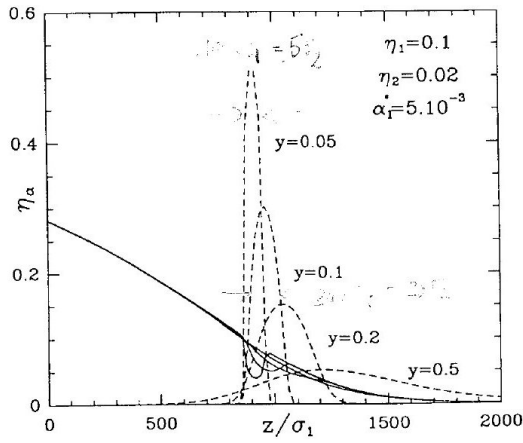
Figure 3.2 shows plots of the density against the reduced height, the light blue dashed line is the calculated density profile from the LDA and the darker blue solid line the Monte-Carlo data. At low altitudes, layering can be seen in the Monte-Carlo data. The LDA does not show this, because it is incapable of describing systems where rapid fluctuations of the density occurs. At altitudes above the layering, the LDA and MC data are in agreement, showing an exponential decay of the density at high altitudes and low density. Because the gravity in figure 3.2(b) is higher than that of 3.2(a), the profile is more compact and shows more layers.

Comparing our figures to figure 3.1, we see that they match very well. Thus we can conclude that for a one component fluid, our work is in agreement with literature.

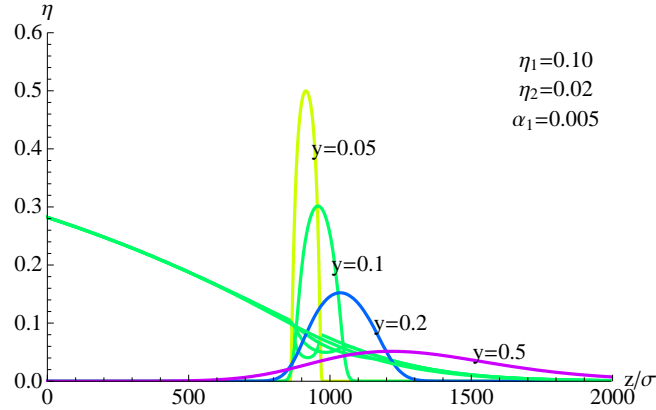
3.1.2 Binary

Next we compare our work on binary mixtures to the available literature. The article to which we compare this work is from Biben and Hansen [3], who performed LDA calculations on this subject. The theory we use is the same as that of Biben, so the set of equations solved is the same, however, we use a different method to solve the equations. The method used by Biben *et al.* is to rewrite equations 2.30 and 2.31 into differential equations and then use a Runge-Kutta method to solve the coupled set of differential equations, while we use an iterative method as described in section 2.2.

Below, our data can be seen in figure 3.3(b) and that of Biben in figure 3.3(a).



(a) Biben's results



(b) Our results

Figure 3.3: Packing fraction profiles $\eta_\nu = \pi \rho_\nu(z) \sigma_\nu^3 / 6$, against reduced altitude z/σ_1 , for small ($\nu = 1$, full curves) and large ($\nu = 2$, dashed curves) spheres; the mean packing fractions are $\eta_1 = 0.1$, $\eta_2 = 0.02$; the reduced gravitational parameter is $\alpha_1^* = 5 \times 10^{-3}$; solutions of the LDA equations are shown for size ratios $y = 0.5, 0.2, 0.1$ and 0.05 .

In the figures the packing fraction can be seen as a function of reduced

height z/σ_1 . The small particles are indicated with the green lines and the large particles by the colored lines. The large particles do not form a profile independent from the small particles, as an ideal gas would, but the interaction can be clearly seen by the forming of a peaked (Gaussian) density profile. The parameter $y = \sigma_1/\sigma_2$ is a parameter that determines the size ratio of the particles. For a large size ratio, the particles float at a higher position and have a broader distribution. Biben also incorporates the size ratio in the equation that determines the mass ratio of the particles.

$$\frac{m_1}{m_2} = \gamma \left(\frac{\sigma_2}{\sigma_1} \right)^3 \frac{\eta_1}{1 - \eta_2(1 + y)^3} \quad (3.1)$$

In the table below the relative mass and relative mass densities are given with the figure parameters for several values of the size ratio y .

Size ratio (y)	Mass ratio (m_1/m_2)	Mass density ratio ($(m_1\sigma_2^3)/(m_2\sigma_1^3)$)
0.5	0.857909	0.107239
0.2	12.9475	0.10358
0.1	102.735	0.102735
0.05	818.961	0.10237

It is clear from the table that while the absolute mass differences vary enormously, the relative mass densities are pretty constant at around 0.10-0.11. The large particles have a lower mass density than the small particles, thus it comes as no surprise that they float, even though they are usually much heavier than the smaller particles. If both species were ideal gasses instead of hard spheres, the large particles would be lower because of their higher mass, the hard sphere interaction insures the mass density becomes more important. Also, since the resulting mass densities from equation 3.1 do not vary much, we do not use it and prefer to vary the size and mass ratios independently.

3.1.3 Monte Carlo simulations on these parameters

As a final confirmation of the LDA model, Monte Carlo simulations have also been done. The results are shown in figure 3.4.

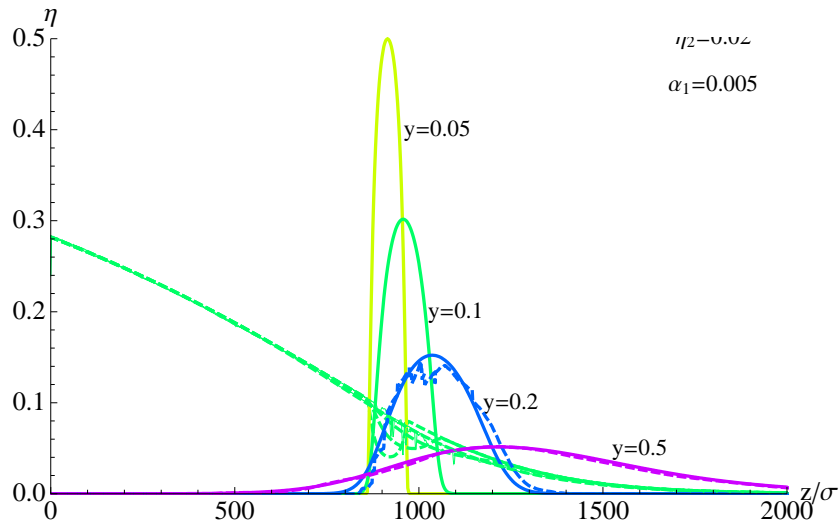


Figure 3.4: Packing fraction profiles from Biben are the solid lines, Monte Carlo profiles are the dashed lines. There are no MC profiles for $y = 0.1, 0.05$

Because of the huge number of particles involved for these specific parameters, only two out of the four profiles were reproduced with the Monte Carlo simulations, namely those with a size ratio $y = 0.5$ and $y = 0.2$. The other size ratios involved both more particles and higher densities, slowing thermalisation down to a crawl. The length of the sides of the box would have to be doubled or quadrupled, and also would the moves from the large particles be rejected more. However, for the two profiles that were determined, they match decently. So we conclude that our Monte Carlo simulations match with literature.

3.1.4 Monte Carlo confirmation for more accessible parameters

Because the parameters used in the calculations by Biben and Hansen require a large number of particles (about forty thousand), Monte Carlo simulations are rather slow in that situation. Therefore simulations and calculations were done with parameters that require less particles. Most notably, the inverse gravitational length α_1 was increased by a factor 10. A series of measurements were done at varying relative mass densities, namely 0.1, 0.2 and 0.3. Two size ratios were used, $y = 0.5$ and $y = 0.3$. For every combination of relative mass and size ratio, the gravity α_1 was increased from 0.05 to 0.20 with steps of 0.05. The results can be seen in figure 3.5. The solid lines are the LDA calculations, green represents the small particles and yellow, green, blue and purple represent the large particles for gravities of 0.05 through 0.20 respectively. The Monte Carlo simulations are represented by the dashed green lines for the small particles and the dashed blue lines for the large particles. The average packing fraction of the small particles was set to 0.1. The packing fraction of the large particles was chosen in such a way that there was only one large particle present in the simulations.

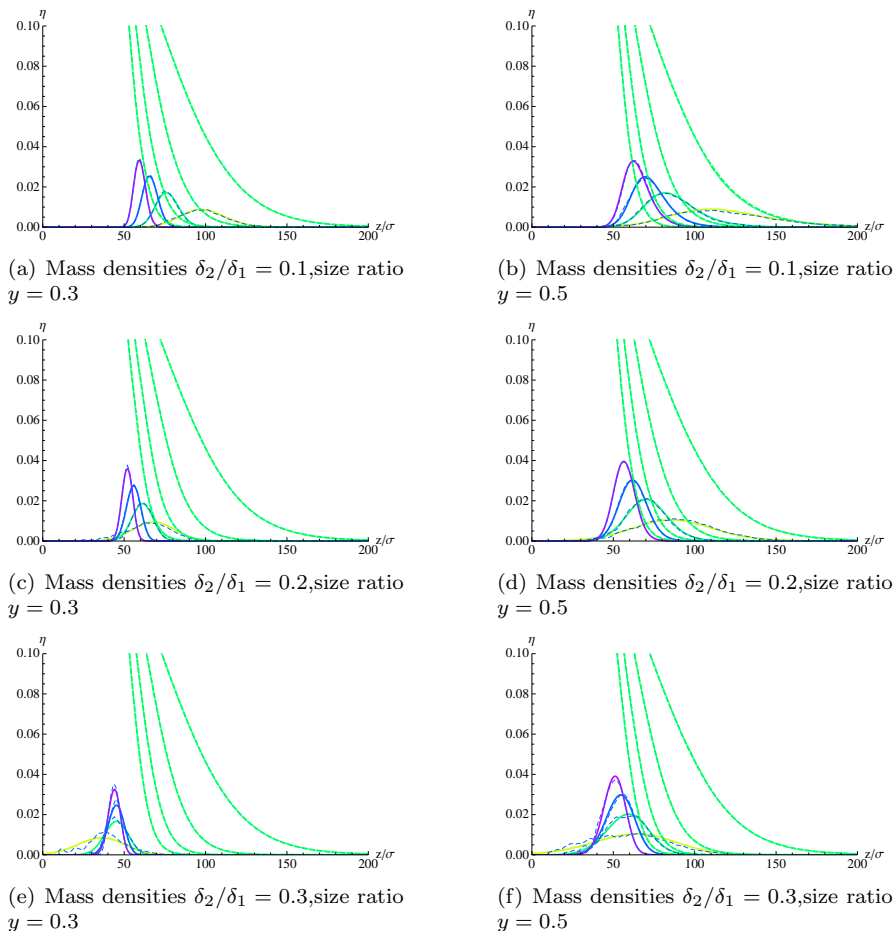


Figure 3.5: Several packing fraction profiles for varying values of relative mass density δ_2/δ_1 and size ratio y . In every figure α_1 runs (right to left) from 0.20 to 0.05. The LDA and MC curves match closely, so are often distinguishable.

In all of the 24 above calculation-simulation pairs, the resulting packing fraction profiles match. The profiles at a relative mass density of 0.3 might not overlap as well as the others, but a longer run time should smooth out the wiggles. From these figures we can conclude that our LDA matches with the MC simulations when the relative mass densities are of the order of 0.1. Also can we conclude that the LDA, which does not treat particle on an individual basis, but rather is a profile, gives accurate packing fraction profiles even in the case of only one large particle, and therefore can be safely used to test the results of the test particle theory.

3.2 Test particle theory

In this section we will take a look at the results from the test particle theory in section 2.1. The two results that are easiest to check are equations 2.9 and 2.15. Only LDA calculations are used for this, because we have already de-

terminated that the Monte-Carlo simulations give the same results as the LDA calculations. LDA calculations are preferred for this analysis, since they are much faster. These LDA calculations take about an hour, while corresponding MC simulations will take up to a year.

$$\tilde{\delta} = (1 - \eta_1(z))\delta_s + \eta_1(z)\delta_1 \quad (3.2)$$

$$\sigma = \sqrt{\frac{k_B T}{m_1 g \tilde{v} |\rho'_1(z^*)|}} \quad (3.3)$$

Equation 3.2 can be rewritten into the following condition

$$\eta_1(z) = \frac{\delta_2}{\delta_1} \frac{1}{(1+y)^3} \quad (3.4)$$

using $\tilde{\delta} = \delta_2 \frac{1}{(1+y)^3}$ (definitions) and $\delta_s = 0$ (equivalent to $\delta_i - \delta_s \rightarrow \delta_i$) and the same can be done to equation 3.3 resulting in

$$\sigma = \sqrt{\frac{1}{\alpha_1 (1 + 1/y)^3 |\eta'_1(z^*)|}} \quad (3.5)$$

All input variables for these equations are calculation parameters, with the exception of $\eta_1(z)$ and $\eta'_1(z^*)$. The derivative was introduced in the theory under the assumption that the small particle profile is unperturbed, therefore it is determined by calculating a profile in absence of large particles. The derivative now only depends on small particle parameters.

3.2.1 Checking the theory against LDA calculations

To see whether the obtained equations made sense, LDA calculations were performed for varying values of α_1 and y at a constant mass density ratio of $\delta_2/\delta_1 = 0.1$. The average packing fraction of the small particle was $\eta_1 = 0.100$ and $\eta_2 = 0.001$ for the large particles. The values of $\alpha_1 = 0.005, 0.010, 0.015, 0.020$ and y was varied between 0.06 and 0.5 with a step size of 0.01. The results of this calculation can be seen in figure 3.6.

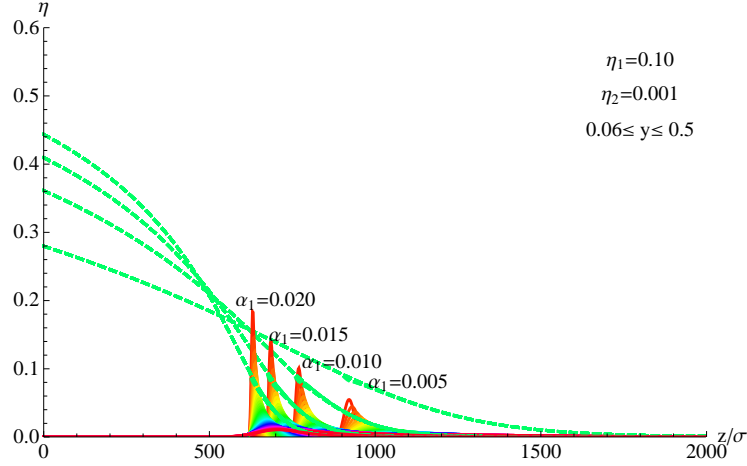


Figure 3.6: LDA packing fractions for four different values of α_1 . for every value of α_1 , the size ratio y was increased from .06 to 0.5 in steps of 0.01

The packing fraction is plotted against the reduced height z/σ_1 . For every value of α_1 , a rainbow colored subseries of peaks can be discerned, these are the packing fractions of the large particles, the green lines are that of the small particles. For higher gravity, the small particle density profiles are shifted to the left, which then shifts the peaks of the large particles to the left as well.

The test particle theory predicts a Gaussian profile for the large particles. These fit the calculated data very well, so we can extract a position and width from the fits with confidence. For every value of α_1 , the position and width of the profiles is plotted against the size ratio. From there, we can check the data easily with equations 3.4 and 3.5.

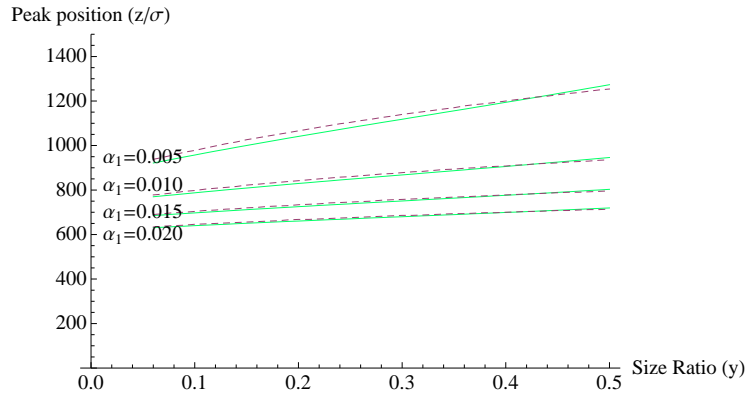


Figure 3.7: Peak position against the size ratio for several values of α_1 . The dashed lines are the predictions from the theory, the solid lines are from the fits to the LDA.

In figure 3.7 the peak position is plotted against the size ratio for several values of α_1 . With increasing y , the peak position also shifts upward, showing that the effective mass density is lowered somewhat.

The lines are very close, so we can conclude that for these variables, the test particle theory accurately gives the peak position.

Next we test the accuracy of equation 3.5. In figure 3.8 the profile width is plotted against the size ratio.

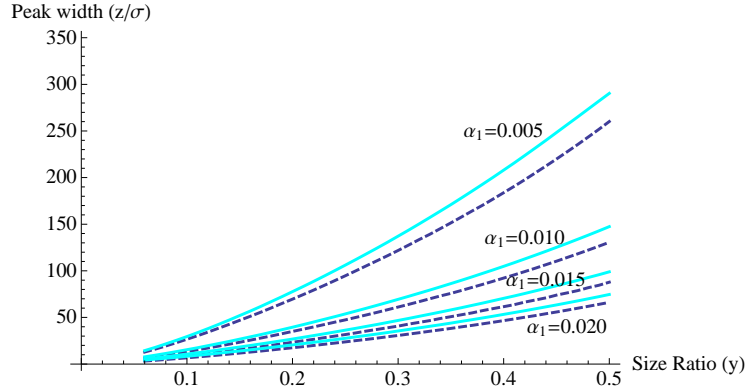


Figure 3.8: Peak width against size ratio for several values of α_1 . The dashed lines are the predictions from the theory, the solid lines are from the fits to the LDA.

The test particle theory underestimates the width for all values of y . The values are pretty close and the shape of the curve is also correct. So while the theory does not exactly match the fitted data, it gives a good indication.

3.2.2 Limits of the test particle theory

When the large particles are light enough to float on top of the smaller particles, the test particle theory can predict the peak position accurately. To see whether the theory remains accurate once the large particles become heavier and start sedimenting on the bottom, a series of LDA calculations was done for increasing relative mass density. The parameters used were $\eta_1 = 0.10$, $\eta_2 = 0.02$, $\alpha_1 = 0.005$, $y = 0.2$ and the relative mass density was increased from 0.1 to 0.35 in steps of 0.05. At a relative mass density of 0.1, the large particles clearly float on top and at 0.35, they have practically reached the bottom. The resulting packing fraction profiles can be seen in figure 3.9.

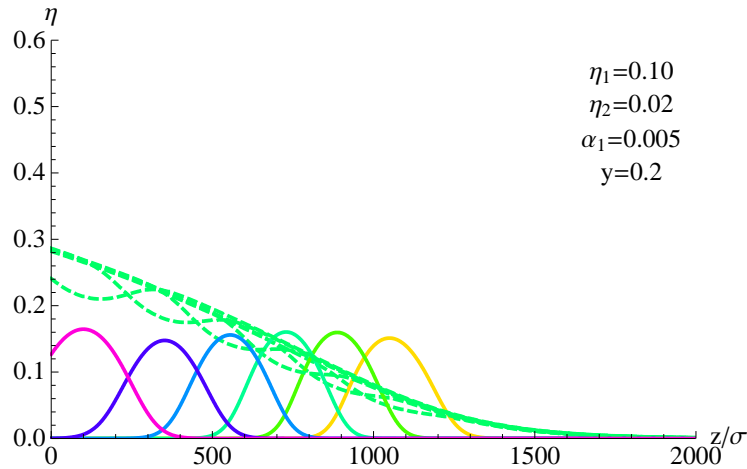


Figure 3.9: A series of density profiles for varying relative mass densities, calculated with the LDA

For every profile, a gaussian was fitted and the peak position was determined. In figure 3.10 these position are plotted against the relative mass density and represented by the solid green line. The dashed blue line is determined by solving equation 3.4 for z and gives the predictions for the peak position according to the test particle theory.

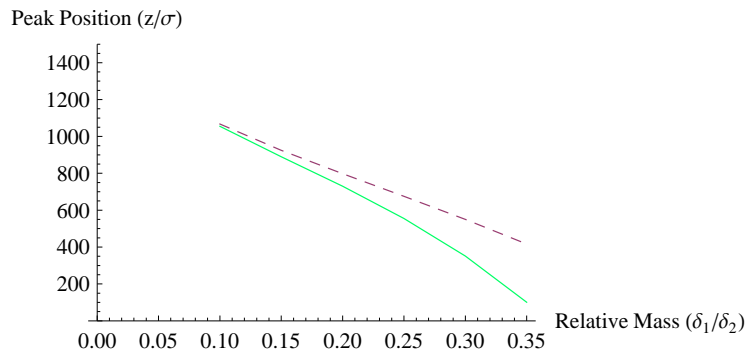


Figure 3.10: Peak position against relative mass density. The dashed lines are the predictions from the theory, the solid lines are from the fits to the LDA.

From figure 3.10, it is clear that for relative mass densities below 0.2, the test particle theory is pretty accurate, while for values above 0.2 the theory becomes increasingly less accurate. This is because we use an adjusted mass density for the large particle which is always lower than the actual mass density. Not using this adjusted mass density will result in a lower peak position, but removes the dependence on the size ratio, which is evident from figure 3.7. So for a higher relative mass density, our theory is no longer accurate. This is because we assume that the excluded volume per particle is given by $\tilde{v} = \frac{4\pi}{3}(a_1 + a_2)^3$. For higher relative mass densities, the larger particles sink lower and the packing fraction increases. At these packing fractions, overlap of excluded volume may

occur and a restructuring of the small particles around the large particles is likely. These effects are not captured in our simple theory and are most likely the causes for the discrepancy.

3.3 Results and limits of the simpler theory

In this section I will show calculations done to compare the simpler DFT from section 2.3 with that in which the more extensive chemical potential is used. The first test was done with the parameters from section 3.1.

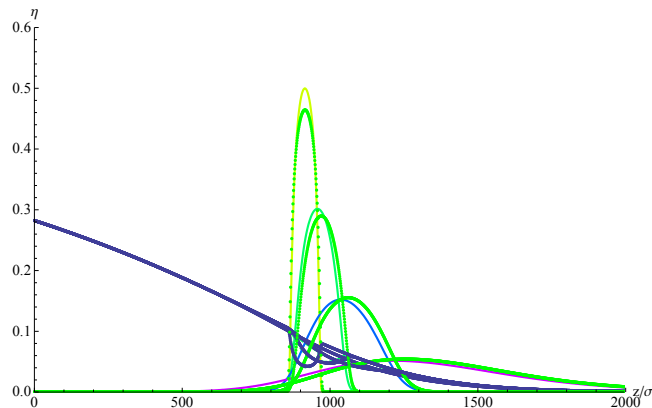


Figure 3.11: Packing fraction profiles η versus reduced height z/σ for y -values of 0.5, 0.2, 0.1 and 0.05. The colored lines are the data from a full treatment and the thick green (dotted) lines are from the simple theory

As can be seen in figure 3.13, the simple theory is pretty accurate for these parameters. The peak position is overestimated a little but the width is spot on. The profiles of the small particles are also matched very well. From the similarity we conclude that for these parameters, the dominant effect which causes the peaked profiles is excluded volume.

From this we can conclude that for parameters where the large particles have a low mass density and the packing fraction of the small particles is low, the assumptions of the simple theory are valid.

According to the test particle theory, the large particle has a lower effective mass density than expected, giving rise to higher peak positions. Here we consider the limit of the situation, where the relative mass densities of both particle species are equal. The size ratio of these particles is $y = 0.5$. This then gives an adjusted mass density of $1/(1 + 0.5)^3 \approx 0.3$. When the packing fraction of the small particles becomes higher than 0.3 at the bottom, we would expect the particle to float according to equation 2.9. To test this we compared it to the full LDA theory and Monte Carlo simulations. The resulting profiles can be seen in figure 3.12.

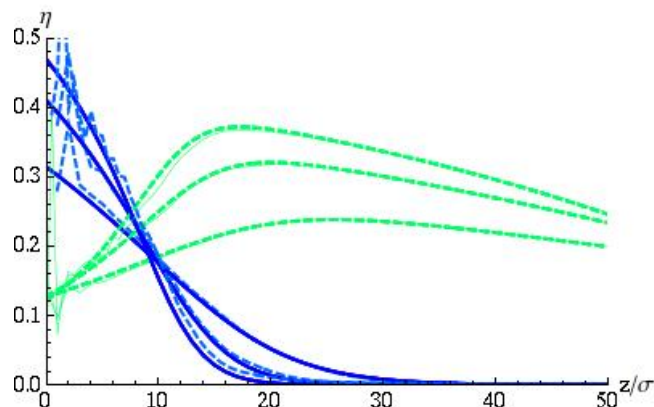


Figure 3.12: $\eta_1 = 0.1$, $\eta_2 = 0.02$, $\alpha_1 = 0.05, 0.10, 0.15$ and 0.20 Relative mass density is 1.0

The green lines in figure 3.13 are the small particle profiles, the blue lines represent the larger particles. At the bottom of the simulation box, due to layering, the LDA and Monte Carlo do not entirely agree, but they do agree that the larger particles do not float. So for this particular case, the test particle theory is not correct.

Next we consider the simpler DFT theory for the same set of parameters. The resulting packing fractions are plotted along with the LDA results in figure 3.13.

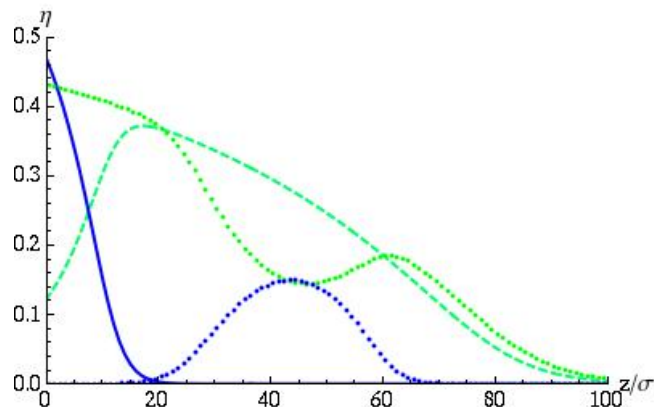


Figure 3.13: $\eta_1 = 0.1$, $\eta_2 = 0.02$, $\alpha = 0.15$. Relative mass density is 1.0 Dotted lines are the simple DFT profiles, solid lines are the LDA profiles. The large particles in blue, small particles in green.

It is clear that the simple DFT also fails at these parameters. As the simplified DFT theory and the test particle theory both use the same excluded volume and rely on the one component Carnahan Starling chemical potential, it is unsurprising that they agree to disagree.

3.4 Comparison with Biesheuvel

Maarten Biesheuvel argues that the effect of floating particles is best described by making the buoyant mass dependent on position, by taking a pressure term into account [12]. From our point of view, we do not have to consider this varying buoyant mass, because we do not use the chemical potential under constant pressure. Thus our chemical potential also takes into account the pressure effects that Biesheuvel thinks are so important. We have tried to produce some data from the article from Biesheuvel. He distinguishes two cases. One where the excess chemical potential - or volume effect as he calls it - is not considered and another where he does use a hard sphere chemical potential to describe volume effects, but it is unclear how he takes care of the constant pressure. Here we only consider calculations with the volume effects, since calculations without give very, very odd results.

To produce some datasets with his equations, the LDA program was adapted to solve another set of equations. The chemical potential used was the same as for our LDA calculations, since Biesheuvel states to use the same chemical potential. The difference between the equations lies in the gravity term. In equation 2.25 our buoyant mass m_i is replaced by his m_i^b . In order to keep using the parameter α_1 independently of height, a factor m_i^b/m_i was included to account for the change in model. The conversion from Biesheuvel's mass to our parameters can be seen in equations 3.6 and 3.7.

$$m_1^b = m_1 \left(1 - \eta_1 - \frac{v_1 m_2}{v_2 m_1} \eta_2 \right) \quad (3.6)$$

$$m_2^b = m_2 \left(1 - \eta_2 - \frac{v_2 m_1}{v_1 m_2} \eta_1 \right) \quad (3.7)$$

In figure 3.14 packing fraction profiles are plotted for the LDA (red), MC (yellow dashed) and Biesheuvel (purple). It is clear that the LDA and MC data overlap and that the calculations with an adapted buoyant mass underestimate the position of the large particles.

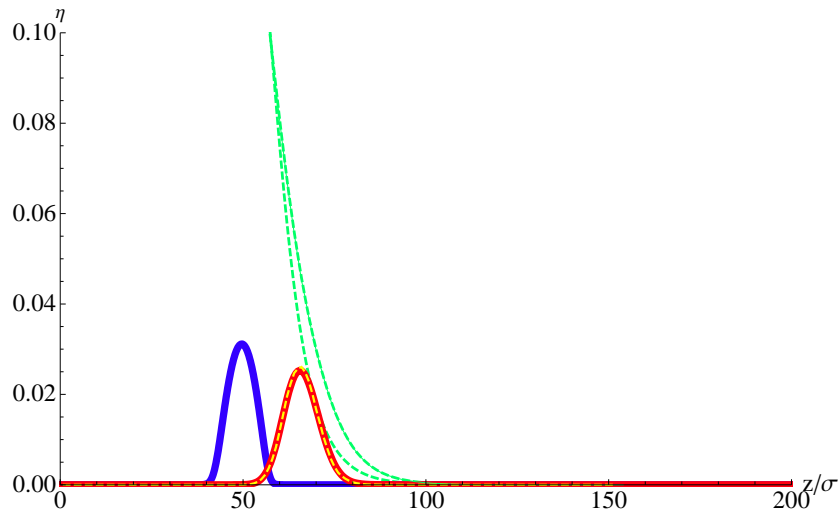


Figure 3.14: Monte Carlo (yellow dashed), LDA (red) and Biesheuvel (purple) packing fraction profiles for a relative mass of $\frac{\delta_2}{\delta_1} = 0.1$, a size ratio of $y = 0.3$ and $\alpha_1 = 0.05$

From this we conclude that our methods are correct and do not need an adjustment to the mass. Because we have investigated a system without charges, the results can not be directly compared to the results from Biesheuvel's article. However we have tried to produce results using the theory in his article and they fail to match to the Monte Carlo data, where ours does coincide.

Chapter 4

Conclusion

In this thesis, we have studied a binary mixture of hard spheres in gravity. Especially concerning the floating behavior when the large particles have a lower density. We have investigated this by the use of Monte Carlo simulations and density functional theory (using the local density approximation). These two methods were first compared to literature and were shown to match for the non-binary mixture. For the binary mixture, only theoretical results are in the literature. Our LDA matches these and also do the simulations. For all parameters used, the simulations match the calculations.

To further investigate the behavior of the large particles in the sea of smaller particles, we developed two theories. The first assumes a single large particle in a sea of small particles and considers the effects of pressure to obtain equations for the position and width of the large particles. The resulting equations were checked against LDA calculations and were found to be accurate to for floating large particles.

The second theory is another local density approximation, but instead of using the free energy for a binary mixture of hard spheres, it makes the assumption that the interparticle interaction is dominated by an excluded volume effect. The resulting density profiles were again found to match for when the large particles float. From this we can conclude that the excluded volume effect is dominant for the behavior of the large particles.

Next we decided to check the limits of these theories and for that we investigated the crossover region, where the large particles start to sediment to the bottom. WE used parameters where the two simplified theories predicted that the large particle would still float. However, using the full LDA and simulations, the large particles were found at the bottom. The simulations and full LDA matches with each other but not with the two simpler theories. Therefore, when the large particles start to sediment, the assumption of excluded volume fails. This is probably caused by a restructuring of the smaller particles around the large particles, which is not included in the theories.

Finally, we have compared our results with the theory that Biesheuvel thinks is the correct way of describing the mixture. We show that our theories differ in a subtle manner and have tried to compare his theory to ours. The data we made using his theory does not match our LDA and also doesn't match the simulations. Therefore we can say that our theory is correct.

Bibliography

- [1] J. Perrin. Mouvement brownien et molécules. *Journal de Physique Théorique et Appliquée*, 9(1):5–39, 1910.
- [2] T. Biben, J.P. Hansen, and J.L. Barrat. Density profiles of concentrated colloidal suspensions in sedimentation equilibrium. *The Journal of Chemical Physics*, 98:7330, 1993.
- [3] T. Biben and J.P. Hansen. Localized density profiles in binary colloidal suspensions. *Molecular Physics*, 80(4):853–859, 1993.
- [4] A. Mori, S. Yanagiya, Y. Suzuki, T. Sawada, and K. Ito. Monte Carlo simulation of crystal-fluid coexistence states in the hard-sphere system under gravity with stepwise control. *The Journal of chemical physics*, 124:174507, 2006.
- [5] H. Chen and H. Ma. The density profile of hard sphere liquid system under gravity. *The Journal of chemical physics*, 125:024510, 2006.
- [6] R. Piazza, T. Bellini, and V. Degiorgio. Equilibrium sedimentation profiles of screened charged colloids: A test of the hard-sphere equation of state. *Physical review letters*, 71(25):4267–4270, 1993.
- [7] MA Rutgers, JH Dunsmuir, J.Z. Xue, WB Russel, and PM Chaikin. Measurement of the hard-sphere equation of state using screened charged polystyrene colloids. *Physical Review B*, 53(9):5043–5046, 1996.
- [8] J.P. Hoogenboom, P. Vergeer, and A. van Blaaderen. A real-space analysis of colloidal crystallization in a gravitational field at a flat bottom wall. *The Journal of Chemical Physics*, 119:3371, 2003.
- [9] P.M. Biesheuvel, H. Verweij, and V. Breedveld. Microdivers to study sedimentation in polydisperse, concentrated colloidal suspensions. *AIChE Journal*, 47(9), 2001.
- [10] GA Mansoori, NF Carnahan, KE Starling, and TW Leland Jr. Equilibrium thermodynamic properties of the mixture of hard spheres. *The Journal of Chemical Physics*, 54:1523, 1971.
- [11] R. Krishna and JA Wesselingh. The Maxwell-Stefan approach to mass transfer. *Chemical Engineering Science*, 52(6):861–911, 1997.

- [12] PM Biesheuvel and J. Lyklema. Sedimentation-diffusion equilibrium of binary mixtures of charged colloids including volume effects. *Journal of Physics, Condensed Matter*, 17(41):6337–6352, 2005.
- [13] N. Metropolis, A.W. Rosenbluth, M.N. Rosenbluth, A.H. Teller, E. Teller, et al. Equation of state calculations by fast computing machines. *The journal of chemical physics*, 21(6):1087, 1953.
- [14] M.E.J. Newman and GT Barkema. *Monte Carlo methods in statistical physics*. Oxford University Press, USA, 1999.